Strangeon matter and strangeon stars in a linked bag model

Zhi-Qiang Miao[1] (ID), Cheng-Jun Xia[2,3] (ID),* Xiao-Yu Lai[4] (ID),
Toshiki Maruyama[3], Ren-Xin Xu[5,6] (ID),† and En-Ping Zhou[7] (ID)

[1]*Department of Astronomy, Xiamen University, Xiamen, Fujian 361005, China*
[2]*School of Information Science and Engineering,*
Zhejiang University Ningbo Institute of Technology, Ningbo 315100, China
[3]*Advanced Science Research Center, Japan Atomic Energy Agency, Shirakata 2-4, Tokai, Ibaraki 319-1195, Japan*
[4]*Department of Physics and Astronomy, Hubei University of Education, Wuhan 430205, China*
[5]*School of Physics, Peking University, Beijing 100871, China*
[6]*Kavli Institute for Astronomy and Astrophysics, Peking University, Beijing 100871, China*
[7]*Max Planck Institute for Gravitational Physics (Albert Einstein Institute),*
Am Mühlenberg 1, Potsdam-Golm, 14476, Germany
(Dated: August 18, 2020)

Inspired by various astrophysical phenomenons, it was suggested that pulsar-like compact stars may in fact be strangeon stars, comprised entirely of strangeons (quark-clusters with three-light-flavor symmetry) and a small amount of electrons. To examine such possibilities, in this work we propose a linked bag model, which can be adopted for strong condensed matter in both 2-flavoured (nucleons) and 3-flavoured (hyperons, strangeons, etc.) scenarios. The model parameters are calibrated to reproduce the saturation properties of nuclear matter, which are later applied to hyperonic matter and strangeon matter. The obtained energy per baryon of strangeon matter is reduced if we adopt larger quark numbers inside a strangeon, which stiffens the equation of state and consequently increases the maximum mass of strangeon stars. In a large parameter space, the maximum mass and tidal deformability of strangeon stars predicted in the linked bag model are consistent with the current astrophysical constraints. It is found that the maximum mass of strangeon stars can be as large as $\sim 2.5 M_\odot$, while the tidal deformability of a $1.4 M_\odot$ strangeon star lies in the range of $180 \lesssim \Lambda_{1.4} \lesssim 340$. More refined theoretical efforts as well as observational tests to these results are necessary in the future.

I. INTRODUCTION

What is the state of matter if normal baryonic matter is compressed so tightly that baryons come into close contact? This question is not only relevant to low-energy strong force, as in the case of nuclear physics, but also important for us to understand an interesting piece of Nature: the huge and dense lump left behind after a core-collapse supernova when gravity dominates inside an evolved massive star. The density of matter in the lump is extremely high, which may even surpass $5n_0$ in the center region with n_0 being the nuclear saturation density. Two questions are frequently raised in the study of such core-compressed matter [1]: 1. Does deconfinement phase transition take place [2–13]? 2. Does strangeness play an important role [14–27]? Normal atomic nucleus is 2-flavoured (u and d), but "giant nucleus" at supra-nuclear densities may very well lie in the regime of 3-flavours of quarks (u, d, and s). It is thus proposed that the core-collapse compressed matter could actually be strange matter, either strange quark matter (quarks free, e.g., Refs. [28–31]) or strangeon matter (quarks localized almost in a certain unit, called strangeon [32, 33]). In principle, a strangeon is a colorsinglet N_q-quark state with the number of quarks N_q = 6, 9, 12, 12, 15, and 18, which includes same amounts of u, d, and s quarks. Due to the non-observation of those multi-quark states, a strangeon may not be stable or only weakly bound in vacuum according to various investigations [34–41]. However, if strangeons are compressed tightly together, the corresponding strangeon matter may become stable due to the strong attractive interactions [42–44], which could form compact stars called strangeon stars [45]. Astrophysically, observational consequences of strangeon stars show that different manifestations of pulsar-like compact objects could be understood in the regime of strangeon stars [46–51], to be tested by future advanced facilities (e.g., FAST, SKA, and eXTP). Both nucleon matter and strangeon matter can be regarded as strong condensed-matter, simply termed strong matter [45], merely with quark-flavour number being 2 for the former and 3 for the latter.

The properties of strangeons in vacuum (i.e., H-dibaryons, strange tribaryons, etc.) were investigated extensively based on various methods. For example, their masses were obtained with QCD-inspired models, i.e., the MIT bag model [34–37, 52, 53], nonrelativistic quark cluster model [54–57], Skyrme model [58–61], diquark model [38], and so on. In recent years, the properties of H-dibaryons were investigated with lattice QCD close to the physical π mass [39–41]. However, as the number of quarks N_q increases, the numerical cost of lattice QCD grows drastically. Similar situation is expected for nonrelativistic quark cluster model since

---

the number of basises grows exponentially. In such cases, for the sake of simplicity, we adopt the MIT bag model [62] to investigate the 2- and 3-flavoured strong matter in a unified manner, where quarks are assumed to be free in a bag-like hadron (perturbative QCD vacuum inside) but this bag is embedded in QCD vacuum characterized by the bag constant, B. For infinite strong matter with negligible surface effect, the interactions between two or more bags can be accounted for if the bags are connected, i.e., a linked bag model, or a bag crystal model [63]. The dynamics of quark propagation between separated bags would thus introduce effective interactions so that "bags" are condensed in strong-matter. With the model parameters carefully calibrated, as will be shown in this work, the properties of nuclear matter, hyperonic matter, and strangeon matter can be obtained simultaneously based on the linked bag model. Surely we are cautious to make any strong conclusions on the exact states of strong matter at different densities due to the complex nature of non-perturbative QCD. Nevertheless, the phenomenological linked bag model helps, at least for a rough estimation with a clear physical picture.

In this paper, we propose a simple version of linked bag model for strong matter (both 2- and 3-flavored) based on a Fermi-gas approximation. The model parameters will be determined by matching constraints of nuclear matter properties from terrestrial experiments of 2-flavoured nucleon matter. We then extend the model parameters into 3-flavoured matter in a natural way. Further study on strangeon matter is carried out, where the mass-radius relation and tidal deformability of strangeon stars are obtained. The results are then compared with both the mass measurements of massive pulsars and the tidal deformability measured by the event of GW170817.

This paper is organized as follows. In Sec. II, we introduce the basic framework of the linked bag model for both 2- and 3-flavored strong matter, where the model parameters are fixed according to the saturation properties of nuclear matter. The model is then applied to investigate the properties of nuclear matter, hyperonic matter, and strangeon matter in Sec. III. With the obtained equation of states (EOSs), the structures of neutron stars, hyperon stars, and strangeon stars are examined and confronted with astrophysical observations. We draw our conclusions in Sec. IV.

II. THEORETICAL FRAMEWORK

A. The linked bag model

In the linked bag model scenario, we suggest that strong matter is composed of quark bags with radius r_q and quark number N_q. In particular, we assume that the bags arrange themselves in simple cubic lattices. The lattice constant a is related to the baryon number density n by $a = (A/n)^{1/3}$, where $A = N_\text{q}/3$ is the baryon
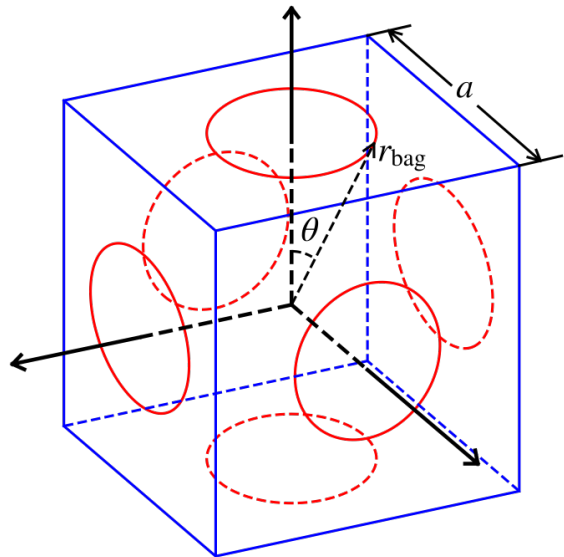

FIG. 1. (Color online) A schematic illustration of a lattice cell in strong condensed-matter, in which point "O" is the center of the cell. A spherical bag (centered at "O" too, not shown) is inside the cell, but the cosine of the angle θ is $\cos\theta = a/(2r_\text{bag})$, with a the lattice constant and r_bag the bag radius. Note that the bag will be linked to other ones through the six windows (the red circles plotted) on the bag's surface.

number of a single bag in a lattice cell. If $r_\text{bag} > a/2$, the bags overlap with each other, and those six parts beyond the cell in Fig. 1 are cut off since they are connected with adjacent cells, leaving behind the main part of the bag with six windows on the surface. The open angle of the window is defined as $\theta = \arccos(a/2r_\text{bag})$. Obviously, the bag surface will disappear when $r_\text{bag} \geq \sqrt{3}a/2$ (i.e., $\theta \geq 54.7°$), implying that the strong matter may go through a phase transition into uniform quark matter. Therefore this linked bag model is different from conventional MIT bag model adopted for strange stars, where we have introduced finite surface structures between bags.

In the Fermi-gas approximation, the energy per lattice cell is obtained with

$$E = \sum_j (\Omega_j + N_j\mu_j) + BV - \frac{z_0}{r_\text{bag}}\frac{\omega}{4\pi}, \quad (1)$$

where Ω_j, N_j and μ_j denote the thermodynamic potential, total particle number, and chemical potential of particle type j. Here after we use j for both quarks and electrons, while i only for quarks, B for the bag parameter, and V for the enclosed volume of the bag. The third term of Eq. (1) looks like the zero-point energy introduced in MIT bag model, which is associated with the quantum fluctuation modes inside the bag and is determined by matching hadron spectra [64]. However, in the linked bag model, we consider z_0 as a parameter to distinguish the difference between the estimated energy

with Fermi-gas approximation and the real value of quark energy, where the variable ω represents the solid angle of the remaining bag. In the extreme case of isolated bags, we have $\omega = 4\pi$ and the dimensionless parameter z_0 is fixed by fitting to hadron spectra. The solid angle ω starts to decrease from 4π when the bags are linked as indicated in Fig. 1. Once r_{bag} reaches $\sqrt{3}a/2$, ω vanishes and the bag takes up the entire volume of the lattice cell with $V = a^3$, i.e., a deconfinement phase transition that restores Eq. (1) into its original MIT bag model description of quark matter. Since we have adopted the Fermi-gas approximation instead of solving the quark single particle energies exactly, the parameter z_0 needs to vary with density to restore the discrete levels, i.e., $z_0 = z_0(n)$. In practice, we fix $z_0(n)$ by reproducing the saturation properties of nuclear matter.

Due to the finite-sized structure of the linked bag, the surface and curvature contributions to quark energy should be taken into account, i.e.,

$$\Omega_i = \Omega_{i,V} V + \Omega_{i,S} S + \Omega_{i,C} C, \tag{2}$$

where $\Omega_{i,V}$, $\Omega_{i,S}$ and $\Omega_{i,C}$ are given by [65–68]

$$\Omega_{i,V} = -\frac{g_i}{24\pi^2} \left[\mu_i u_i (\mu_i^2 - \frac{5}{2} m_i^2) + \frac{3}{2} m_i^4 \ln \frac{\mu_i + u_i}{m_i} \right] \tag{3}$$
$$+ \frac{g_i \alpha_s}{12\pi^3} \left[3 \left(\mu_i m_i - m_i^2 \ln \frac{\mu_i + u_i}{m_i} \right)^2 - 2u_i^4 \right.$$
$$\left. + \left(6m_i^2 \ln \frac{\bar{\Lambda}}{m_i} + 4m_i^2 \right) \left(\mu_i u_i - m_i^2 \ln \frac{\mu_i + u_i}{m_i} \right) \right],$$

$$\Omega_{i,S} = \frac{g_i}{8\pi} \left[\frac{\mu_i u_i^2}{6} - \frac{m_i^2(\mu_i - m_i)}{3} - \frac{1}{3\pi} \left(\mu_i^3 \arctan \frac{u_i}{m_i} \right. \right.$$
$$\left. \left. -2\mu_i u_i m_i + m_i^3 \ln \frac{\mu_i + u_i}{m_i} \right) \right], \tag{4}$$

$$\Omega_{i,C} = \frac{g_i}{48\pi^2} \left(m_i^2 \ln \frac{\mu_i + u_i}{m_i} + \frac{\pi}{2} \frac{\mu_i^3}{m_i} - \frac{3\pi \mu_i m_i}{2} + \pi m_i^2 \right.$$
$$\left. -\frac{\mu_i^3}{m_i} \arctan \frac{u_i}{m_i} \right), \tag{5}$$

with $u_i \equiv \sqrt{\mu_i^2 - m_i^2}$ and g_i the degeneracy factor ($g_u = g_d = g_s = 6$) for quark flavor i. The area S and curvature C of the bag are obtained with $S = \omega r_{\text{bag}}^2$ and $C = 2\omega r_{\text{bag}}$, respectively. Note that in Eq. (3) we have considered the first-order correction to the thermodynamic potential of QCD. The coupling constant α_s and quark masses m_i are running with energy scale [65], i.e.,

$$\alpha_s(\bar{\Lambda}) = \frac{1}{\beta_0 L} \left(1 - \frac{\beta_1 \ln L}{\beta_0^2 L} \right), \tag{6}$$

$$m_i(\bar{\Lambda}) = \hat{m}_i \alpha_s^{\gamma_0/\beta_0} \left[1 + \left(\frac{\gamma_1}{\beta_0} - \frac{\beta_1 \gamma_0}{\beta_0^2} \right) \alpha_s \right], \tag{7}$$

where $L = 2\ln(\bar{\Lambda}/\Lambda_{\overline{\text{MS}}})$ and $\Lambda_{\overline{\text{MS}}}$ is the $\overline{\text{MS}}$ renormalization point. In this work we take $\Lambda_{\overline{\text{MS}}} = 376.9$ MeV and $\hat{m}_u = \hat{m}_d = 0$, $\hat{m}_s = 220$ and 280 MeV. The parameters

of β-function and γ-function are $\beta_0 = \frac{1}{4\pi}(11 - \frac{2}{3} N_{\text{f}})$, $\beta_1 = \frac{1}{16\pi^2}(102 - \frac{38}{3} N_{\text{f}})$, $\gamma_0 = 1/\pi$ and $\gamma_1 = \frac{1}{16\pi^2}(\frac{202}{3} - \frac{20}{9} N_{\text{f}})$ with $N_{\text{f}} = 3$ [69]. The renormalization scale envolves with the chemical potentials of quarks, and we adopt $\bar{\Lambda} = \frac{C_1}{3} \sum_i \mu_i$ with $C_1 = 1 \sim 4$ [70].

The bag parameter B was introduced to account for the energy difference between physical vacuum and perturbative vacuum of QCD [62]. Its value was estimated under various circumstances, while we still do not know how exactly does the bag parameter vary with density. According to QCD sum-rule [71], one finds $B \simeq 455$ MeV/fm^3 at vanishing chemical potentials, while fitting to the hadron spectra gives a lower value $B \simeq 50$ MeV/fm^3 [64]. At larger chemical potentials, however, it is found that B prefers a larger value by comparing with the pQCD calculations to higher orders [70]. To account for these values in our current study, we take a third-order expansion of B with respect to ξ, i.e.,

$$B = B_0 + B_1 \xi + B_2 \xi^2 + B_3 \xi^3, \tag{8}$$

where $\xi = (\sum_i N_i \mu_i / A - m_N)/m_N$ with the baryon number of a lattice cell $A = \sum_i N_i/3$ and the nucleon mass $m_N = 938$ MeV. This expansion is composed by three parts: the constant part B_0, the symmetric part $B_2 \xi^2$ and the asymmetric part $B_1 \xi + B_3 \xi^3$. In this work we fix $B = B_0 = 50$ MeV/fm^3 at $\sum_i N_i \mu_i / A = m_N$ ($\xi = 0$), while the first-order term is discarded by taking $B_1 = 0$ so that $\partial B/\partial \mu_i = 0$ at $\xi = 0$. The remaining parameters B_2 and B_3 are left undetermined and will be fixed later. The particle number N_j is then related to the chemical potentials μ_j via

$$N_j = -\frac{\partial \Omega_j}{\partial \mu_j} - \frac{\partial B}{\partial \mu_j} V. \tag{9}$$

The bag radius r_{bag} is then fixed by minimizing the total energy E at a given cell volume a^3 and particle numbers N_i. With the energy per baryon determined by E/A, the energy density reads

$$\varepsilon = nE/A. \tag{10}$$

According to the basic thermodynamic relations, the baryon chemical potential and pressure are obtained with

$$\mu_{\text{b}} = \frac{d\varepsilon}{dn}, \tag{11}$$

$$P = n^2 \frac{d}{dn} \frac{\varepsilon}{n} = n \frac{d\varepsilon}{dn} - \varepsilon = n\mu_{\text{b}} - \varepsilon. \tag{12}$$

B. Model parameters

In our linked bag model, the energy per baryon of both symmetric nuclear matter and neutron matter is obtained by taking $N_u = N_d = 3/2$ and $N_u = N_d/2 = 1$, respectively. At given B_2 and B_3, the model parameters C_1 and $z_0(n_0)$ are fixed by reproducing the saturation

TABLE I. Parameter sets $(C_1, \hat{m}_s, B_2, B_3, z_0(n_0))$ chosen to reproduce saturation properties in nuclear matter: the saturation density $n_0 = 0.16\,\mathrm{fm}^{-3}$, the minimum energy per baryon $E_0(n_0) = 922$ MeV, the incompressibility $K = 240\,\mathrm{MeV}$, the symmetry energy $E_{\mathrm{sym}}(n_0) = 31.7\,\mathrm{MeV}$. consequent symmetry energy slope L (in MeV) is also listed.

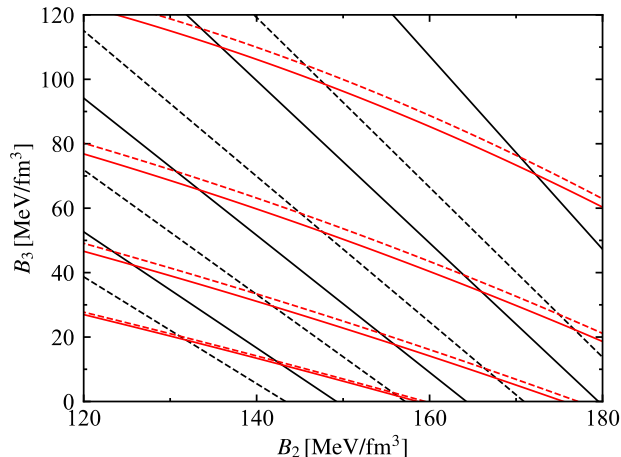|	C_1	$\hat{m}_s[\mathrm{MeV}]$	$B_2[\mathrm{MeV/fm}^3]$	$B_3[\mathrm{MeV/fm}^3]$	$z_0(n_0)$	$L[\mathrm{MeV}]$
(i)	2.7	220	136.7	50	2.944	45.1
(ii)	2.7	220	112.7	100	2.926	52.7
(iii)	2.7	280	125.0	100	2.908	56.6
(iv)	3.2	280	162.3	100	2.843	62.8

FIG. 2. (Color online) The values of B_3 as functions of B_2. The black curves adopt constant values of C_1, with $C_1 = 2.3, 2.6, 2.9, 3.2$ from lower-left to upper-right. Alternatively, the red curves adopt constant values of symmetry energy slope L, with $L = 30, 40, 50, 60$ MeV from lower-left to upper-right. For the solid and dashed curves, two invariant strange quark masses $\hat{m}_s = 280\,\mathrm{MeV}$ and 220 MeV are adopted, respectively.
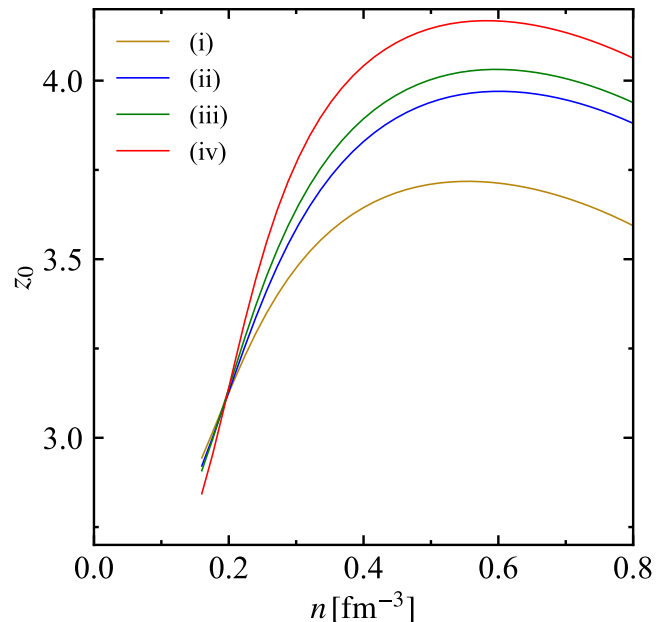

FIG. 3. (Color online) The zero-point parameter as a function of baryon number density for the selected parameter sets listed in Table I.

properties of nuclear matter, while $z_0(n)$ at $n \neq n_0$ is obtained by fitting to the energy per baryon of symmetric nuclear matter. In this work, the energy per baryon of nuclear matter is determined by a parabolic expansion, i.e.,

$$E_{\mathrm{NM}} = E_0(n_0) + \frac{K_0}{2}(\frac{n - n_0}{3n_0})^2 + E_{\mathrm{sym}}(n)\delta^2 \qquad (13)$$

with the symmetry energy

$$E_{\mathrm{sym}}(n) = E_{\mathrm{sym}}(n_0) + L(\frac{n - n_0}{3n_0}). \qquad (14)$$

Here $\delta = (n_n - n_p)/n = N_d - N_u$ represents the isospin asymmetry with n_p and n_n being the proton and neutron number densities. According to various experimental investigations and nuclear theories [72–74], the parameters in Eq. (13) are constrained with the nuclear saturation density $n_0 \approx 0.16\,\mathrm{fm}^{-3}$, the minimum energy per baryon $E_0(n_0) \approx 922$ MeV, the

incompressibility $K_0 = 240 \pm 20\,\mathrm{MeV}$, the symmetry energy $E_{\mathrm{sym}}(n_0) = 31.7 \pm 3.2\,\mathrm{MeV}$ and its slope $L = 58.7 \pm 28.1\mathrm{MeV}$. We thus take their central values with $K_0 = 240\,\mathrm{MeV}$ and $E_{\mathrm{sym}}(n_0) = 31.7\,\mathrm{MeV}$, while several values of L are adopted due to its larger uncertainty.

The parameters C_1 and z_0 are then fixed at given B_2 and B_3. In Fig. 2 we present the constraints on the parameter set (B_2, B_3), where we have taken either C_1 (red curves) or L (black curves) as constant values. According to Fig. 2, in this work we adopt four parameter sets (i-iv) with the corresponding values listed in Table I.

The obtained values of z_0 corresponding to sets (i-iv) are presented in Fig. 3. It is interesting to notice that z_0 increases with density and reaches its peak value at $n \approx 3.5n_0$, which later decreases at larger densities. This may be related to the variations of nucleon structures as well as the strong correlations with neighboring nucleons in nuclear medium, e.g, the EMC effect [75]. However, a more detailed investigation with the single particle energies more accurately determined might be necessary

in the future. In our current study, the obtained nucleon radius is decreasing with density, and is approaching to a constant value at highest densities.

For hyperonic and strangeon matter with $N_q \geq 3$ and $N_s \neq 0$, we adopt the same values of B_0, B_2, and B_3 as indicated in Table I since one would expect that strong interactions do not vary with quark flavor. For the parameter z_0, keeping z_0 unchanged might be reasonable for $N_q = 3$. However, $z_0(n)$ could be different at larger N_q, which contains quark energy level corrections that are approximately proportional to the quark number N_q, i.e., $\frac{z_0}{r_{\rm bag}} \propto N_q$. As a crude estimate, we have $z_0 \propto N_q^{4/3}$ since $r_{\rm bag} \propto N_q^{1/3}$ at fixed number density. In fact, our Fermi-gas approximation overestimates the energy at small N_q with quarks occupying the $1s_{1/2}$ orbit, while this approximation should holds at large enough N_q, i.e., vanishing quark energy level corrections. Under such circumstances, with the parameter $\tilde{z}_0$ obtained by reproducing nuclear matter properties, we fix z_0 with an effective formula $z_0 = (\frac{N_q}{3})^{4/3}\tilde{z}_0 - f$, where a dampening factor f is introduced to account for the reduction of quark energy level corrections. Note that we take $f = 0$ at $N_q = 3$, i.e., $z_0 = \tilde{z}_0$, while larger f may be expected at larger N_q.

III. STRONG MATTER AND COMPACT STARS

A. Properties of nuclear matter, hyperonic matter, and strangeon matter

In this section we study strong matter inside compact stars, which is comprised of bags with quark number N_q. The electrons are included to fulfill the charge neutrality condition

$$\sum_i Q_i N_i + Q_e N_e = 0, \tag{15}$$

where Q_i and Q_e are respectively the charge of quark flavor i and electrons, i.e., $Q_u = 2/3$, $Q_d = Q_s = -1/3$ and $Q_e = -1$. Note that electrons are not confined within the bags, the corresponding thermodynamic potential can then be obtained with

$$\Omega_e = \Omega_{e,\rm V} a^3 = -\frac{\mu_e^4}{12\pi^2} a^3. \tag{16}$$

In principle, μ^- will appear in the centre region of a neutron star. However, we neglect the contribution of μ^- since it becomes insignificant for hyperon stars and strangeon stars.

The quarks and leptons will undergo various weak reactions, i.e.,

$$u + e^- \to d + \nu_e, \quad d \to u + e^- + \bar{\nu}_e. \tag{17}$$

If strangeness is involved (3-flavored matter), the follow-

ing reactions take place, i.e.,

$$u + e^- \to s + \nu_e, \quad s \to u + e^- + \bar{\nu}_e, \tag{18a}$$
$$s + u \leftrightarrow d + u. \tag{18b}$$

Then the β-equilibrium is reached, i.e.,

$$\mu_u + \mu_e = \mu_d = \mu_s. \tag{19}$$

In this work, the β-equilibrium condition is satisfied by minimizing the total energy with respect to the particle numbers N_i at a given total baryon number $A = \sum_i N_i/3 = N_q/3$. Then the energy density and pressure are obtained with Eqs. (10-12), which correspond to the EOS of strong matter. As illustrated in Sec. II B, we keep B unchanged and $z_0 = (\frac{N_q}{3})^{4/3}\tilde{z}_0 - f$ with f being the dampening factor. In this paper, we limit our discussions for strong matter with $N_q = 3$ and $N_q = 9$. Particularly, we take $f = 0$ for $N_q = 3$ and $f = 5.8$ for $N_q = 9$.

In Fig. 4 we present the energy per baryon as well as the EOSs of nuclear matter ($N_q = 3$, $N_s = 0$), hyperonic matter ($N_q = 3$, $N_s \neq 0$), and strangeon matter ($N_q = 9$) in compact stars, which are obtained with the selected parameter sets in Table I. In this work, our model is restricted to describe strong matter at $n \geq 0.16\,{\rm fm}^{-3}$. In the density regime of $n < 0.16\,{\rm fm}^{-3}$, we employ the results of Negele & Vautherin [76] for $0.001\,{\rm fm}^{-3} < n < 0.08\,{\rm fm}^{-3}$, and of Baym et al. [77] for $n < 0.001\,{\rm fm}^{-3}$. Between $0.08\,{\rm fm}^{-3}$ and $0.16\,{\rm fm}^{-3}$, we simply take a linear interpolation since the structures of compact stars are insensitive to the EOSs adopted in this density region. For each parameter set, the energy per baryon of nuclear matter is decreased once s-quarks (hyperons) emerge at about twice the nuclear saturation density. The energy is further reduced if we take $N_q > 3$, i.e., strangeon matter with $N_q = 9$. We notice that strangeon matter reaches its minimum at $2\sim3n_0$. For a few cases, the energy per baryon of strangeon matter can even be smaller than $930\,{\rm MeV}$, namely strangeon matter is more stable than ^{56}Fe. Combined with Fig. 2, we notice that the minimum energy per baryon of strangeon matter increases while the corresponding density decreases along the curves with fixed C_1 from top-left to lower-right regions.

In the right panel of Fig. 4, it is easy to see that the EOSs of strangeon matter are stiffer than that of nuclear matter and hyperonic matter, which indicates that the introduction of linked bag will results in stiffening of EOSs. The energy densities at zero pressure lie between $\sim280\,{\rm MeV/fm}^3$ and $\sim360\,{\rm MeV/fm}^3$, or, equivalently, ~1.8 and ~2.4 times the nuclear saturation density (mass density). It is worth noting that, although the equation of state is very stiff, the causality condition is still satisfied for strangeon matter [78].

B. Structure of neutron stars, hyperon stars, and strangeon stars

The equilibrium configurations of compact stars can be obtained by solving the Tolman-Oppenheimer-Volkoff
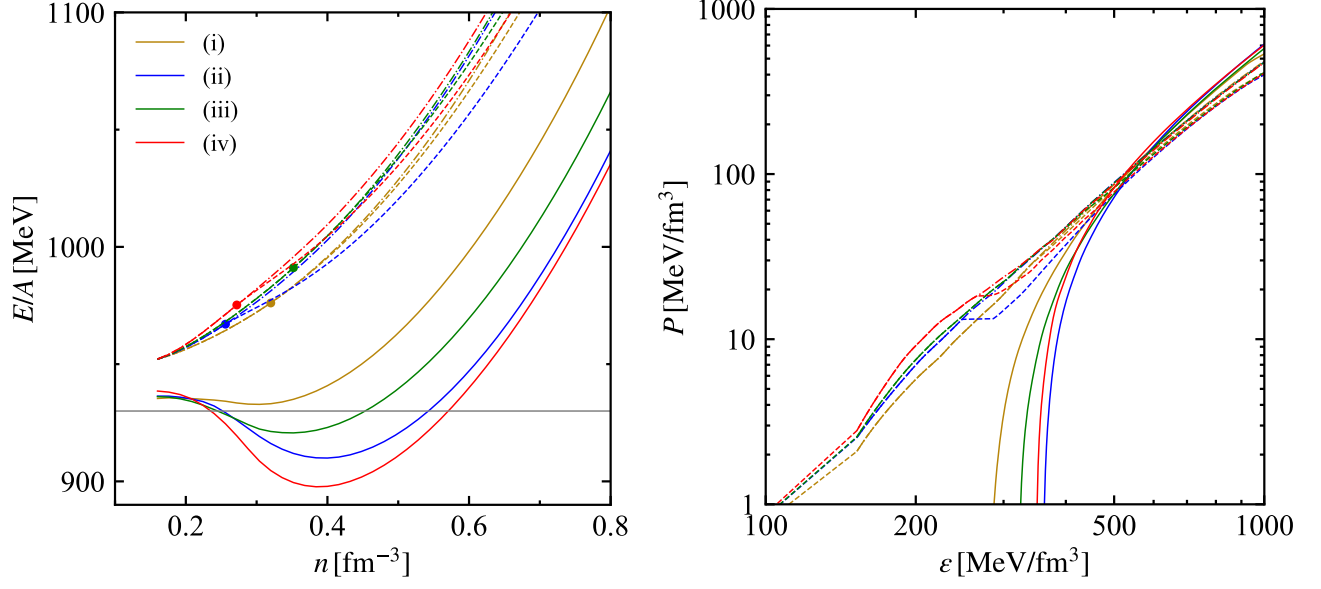
FIG. 4. (Color online) Left: The energy per baryon as a function of density for strong matter obtained with the parameter sets listed in Table I. Right: The corresponding EOS for each case. The obtained results for traditional neutron stars ($N_q = 3$ in dash-dotted lines), hyperon stars ($N_q = 3$ in dashed lines), and strangeon stars ($N_q = 9$ in solid lines) are plotted. For strangeon matter with $N_q = 9$, we take $f = 5.8$. The horizontal line in the left panel corresponds to $E/A = 930\,\mathrm{MeV}$, which is the energy per baryon of the most stable atomic nucleus, ^{56}Fe. The solid dots indicate the critical densities at which s quark starts to appear in hyperon matter.

(TOV) equations for the pressure P and the enclosed mass m, i.e.,

$$\frac{dP(r)}{dr} = -\frac{m(r)\varepsilon(r)}{r^2} \tag{20}$$
$$\times \frac{[1 + P(r)/\varepsilon(r)][1 + 4\pi r^3 P(r)/m(r)]}{1 - 2m(r)/r},$$

$$\frac{dm(r)}{dr} = 4\pi r^2 \varepsilon(r), \tag{21}$$

where $P(r)$ and $\varepsilon(r)$ are the pressure and energy density at the radial coordinate r, respectively. Starting with a central density $\varepsilon(r = 0) \equiv \varepsilon_c$, we integrate out until the pressure on the surface vanishes. This gives the stellar radius R and the gravitational mass, i.e.,

$$M \equiv m(R) = 4\pi \int_0^R dr\, r^2 \varepsilon(r). \tag{22}$$

The Love number k_2 measures how easily a star is deformed by an external tidal field. The tidal deformability λ describes the amount of induced mass quadruple moment Q_{ij} when reacting to a certain external tidal field E_{ij}, i.e., $Q_{ij} = -\lambda E_{ij}$. The dimensionless tidal deformability is related to the Love number k_2 through $\Lambda = \frac{2}{3}k_2 c^{-5}$, where $c = M/R$ is the compactness of the star. The Love number is given by

$$\begin{aligned} k_2 =& \frac{8c^5}{5}(1 - 2c)^2[2 + 2c(y_R - 1) - y_R] \\ &\times \{2c[6 - 3y_R + 3c(5y_R - 8)] \\ &+ 4c^3[13 - 11y_R + c(3y_R - 2) + 2c^2(1 + y_R)] \\ &+ 3(1 - 2c)^2[2 - y_R + 2c(y_R - 1)]\ln(1 - 2c)\}^{-1}, \end{aligned} \tag{23}$$

where $y_R = y(R)$ is obtained by solving the following differential equation:

$$r\frac{dy(r)}{dr} + y(r)^2 + y(r)F(r) + r^2 Q(r) = 0, \tag{24}$$

with

$$F(r) = \{1 - 4\pi r^2[\varepsilon(r) - P(r)]\}[1 - \frac{2m(r)}{r}]^{-1}, \tag{25}$$

$$\begin{aligned} Q(r) =& 4\pi[5\varepsilon(r) + 9P(r) + \frac{\varepsilon(r) + P(r)}{\partial P(r)/\partial \varepsilon(r)} - \frac{6}{4\pi r^2}] \\ &\times [1 - \frac{2m(r)}{r}]^{-1} - \frac{4m(r)^2}{r^4}[1 + \frac{4\pi r^3 P(r)}{m(r)}]^2 \\ &\times [1 - \frac{2m(r)}{r}]^{-2}. \end{aligned}$$

Note that the solution $y(r)$ will be altered in case of density discontinuity by $y^{\mathrm{out}}(r_d) = y^{\mathrm{int}}(r_d) - \frac{\Delta\varepsilon}{4\pi m(r_d)/r_d^3}$, r_d is the radius of discontinuity point and $\Delta\varepsilon$ is the energy density jump. Such situation is expected on the
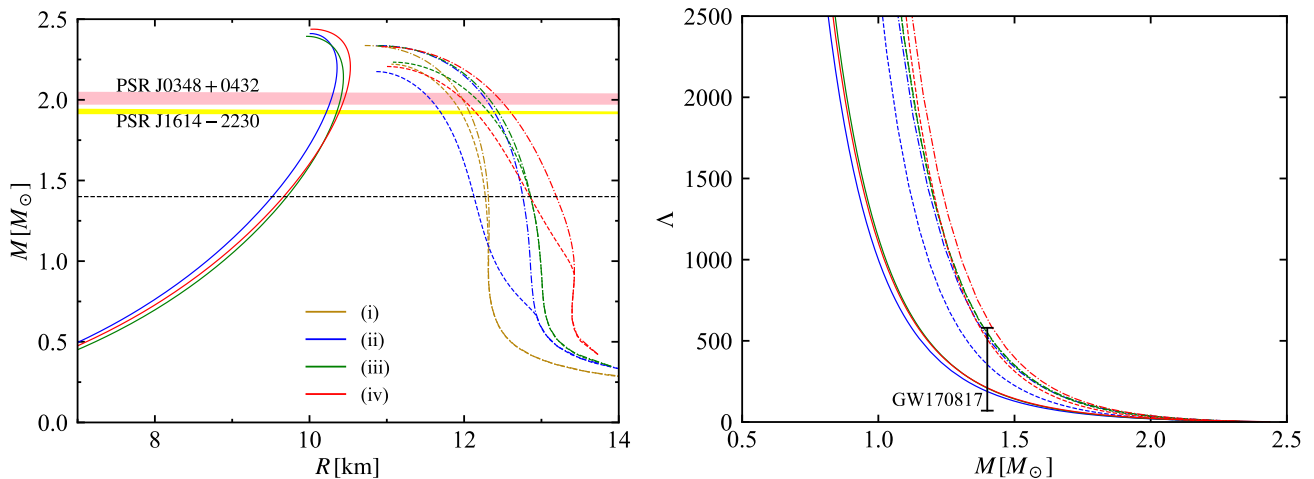
FIG. 5. (Color online) Mass-radius relations (left panel) and tidal deformability as a function of stellar mass (right panel). The obtained results for traditional neutron stars ($N_q = 3$ in dash-dotted lines), hyperon stars ($N_q = 3$ in dashed lines), and strangeon stars ($N_q = 9$ in solid lines) are plotted. For strangeon stars with $N_q = 9$, we take $f = 5.8$. The observational masses of PSR J1614-2230 ($1.928 \pm 0.017\,M_\odot$) [79, 80] and PSR J0348+0432 ($2.01 \pm 0.04\,M_\odot$) [81] are indicated with horizontal bands. The horizontal dashed lines correspond to $M = 1.4\,M_\odot$. The the LIGO/Virgo constraint [82] from GW170817 on the tidal deformability for a $1.4\,M_\odot$ star, $\Lambda_{1.4} = 190^{+390}_{-120}$, is also displayed in right panel.
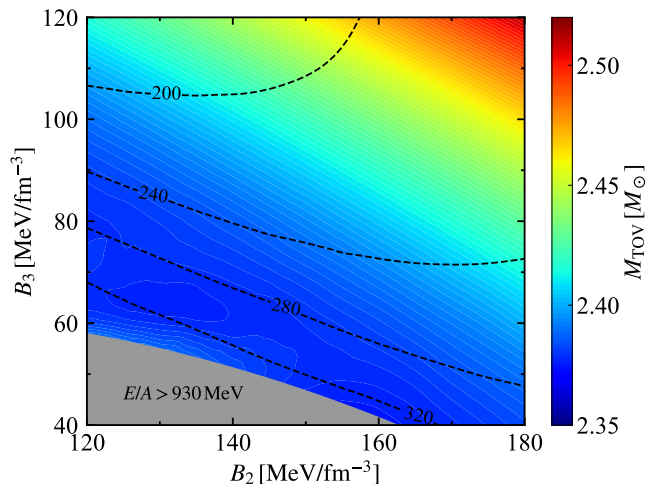

FIG. 6. (Color online) Maximum mass M_{TOV} and tidal deformability of a typical $1.4\,M_\odot$ star ($\Lambda_{1.4}$) for strangeon stars with $N_q = 9$. The invariant strange quark mass is $\hat{m}_s = 280\,\mathrm{MeV}$. Contours of M_{TOV} are illustrated in colors, while contours of $\Lambda_{1.4}$ are plotted in black dashed lines. The lower-left grey region is ruled out since strangeon matter becomes unstable with the minimum energy per baryon $E/A > 930\,\mathrm{MeV}$.

surfaces of strangeon stars at $r_d = R$, where the energy density vanishes with $\varepsilon(R_+) = 0$ and $\Delta\varepsilon = \varepsilon(R_-)$.

Based on the EOSs presented in Fig. 4, the mass-radius relations of compact stars are obtained by solving Eqs. (20-22), while the tidal deformability is determined by Eqs. (23-26). The results are presented in Fig. 5, where various parameter sets listed in Table I are

adopted. The corresponding properties of strangeon stars are listed in Table II. In general, the maximum masses of strangeon stars are higher than those of neutron stars and hyperon stars due to the stiffer EOSs of strangeon stars. It is shown that the radius of a typical $1.4\,M_\odot$ star ranges from $9.5\,\mathrm{km}$ to $13\,\mathrm{km}$, where strangeon stars with $N_q = 9$ have smaller radii and larger maximum mass than those with $N_q = 3$. In right panel of Fig. 5, we find Λ decreases monotonously with mass. Except for the traditional neutron star obtained with parameter set (iv), the tidal deformability of a typical $1.4\,M_\odot$ star $\Lambda_{1.4}$ is found between about 190 and 550 for all presented cases, which fulfills the GW170817 constraint of $\Lambda_{1.4} < 580$ [82].

To investigate the effects of different parameters more carefully, in Fig. 6 we present contours of maximum mass and tidal deformability for strangeon stars. It is found that the maximum mass increases with B_2 and B_3, which even exceeds $2.5\,M_\odot$ in the top right corner. In light of the recent measured massive compact object (2.50-$2.67\,M_\odot$) in a compact binary coalescence of GW190814 [83], the object may in fact be a strangeon star instead of a black hole. Meanwhile, even in the lower left corner, the maximum mass remains higher than $2\,M_\odot$, which fulfills the recent observational constraints of two massive stars: PSR J1614-2230 ($1.928 \pm 0.017\,M_\odot$) [79, 80] and PSR J0348+0432 ($2.01 \pm 0.04\,M_\odot$) [81]. Since the central densities of $1.4\,M_\odot$ strangeon stars are much smaller than the most massive stars, the tidal deformability $\Lambda_{1.4}$ is somewhat insensitive to B_2 and B_3, while $\Lambda_{1.4}$ is decreasing slightly with B_3. In the parameter space indicated in Fig. 6, $\Lambda_{1.4}$ ranges from ~ 180 to ~ 340, which fulfills the GW170817 constraint [82].

In the discussions above, we have fixed $f = 5.8$

TABLE II. The surface baryon number ($n_{\rm surf}$) and energy ($\varepsilon_{\rm surf}$) densities, radius ($R_{1.4}$), tidal deformability ($\Lambda_{1.4}$), TOV mass ($M_{\rm TOV}$), and centre baryon number density ($n_{\rm c}$) for strangeon stars obtained with the parameter sets listed in Table I.

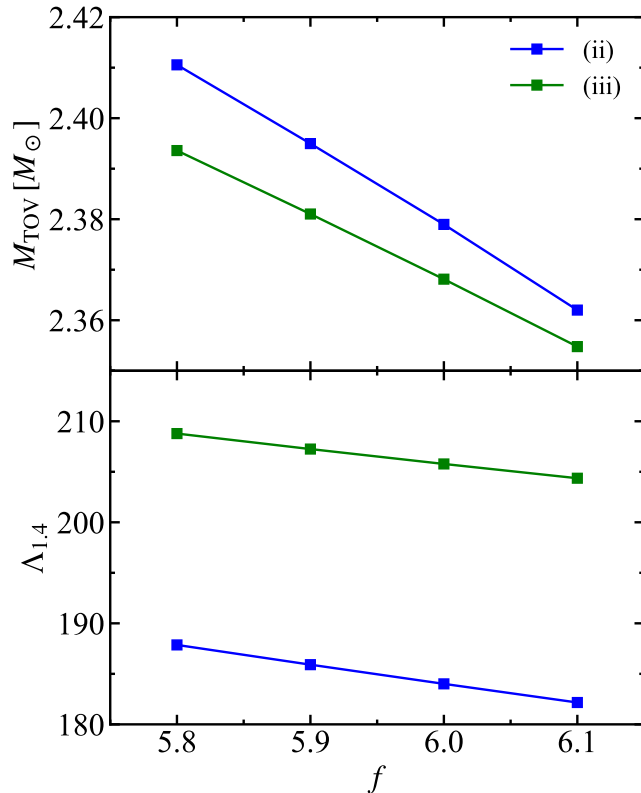|	$n_{\rm surf}[{\rm fm}^{-3}]$	$\varepsilon_{\rm surf}[{\rm MeV/fm}^3]$	$R_{1.4}[{\rm km}]$	$\Lambda_{1.4}$	$M_{\rm TOV}[M_\odot]$	$n_{\rm c}[{\rm fm}^{-3}]$
(ii)	0.395	359.38	9.519	187.9	2.411	1.069
(iii)	0.348	320.56	9.710	208.8	2.394	1.086
(iv)	0.388	348.11	9.666	210.4	2.438	1.080

FIG. 7. (Color online) Maximum mass M and tidal deformability ($\Lambda_{1.4}$) of strangeon stars as functions of the dampening factor f.

for strangeon stars with $N_{\rm q} = 9$. However, f is a free parameter introduced to denote the energy level correction and the exact value of f is unknown. It is thus meaningful to investigate the effects of f on strangeon star structures. For this reason, in Fig. 7 we present the maximum mass M and tidal deformability ($\Lambda_{1.4}$) of strangeon stars as functions of the dampening factor f. In general, the maximum mass and tidal deformability monotonously decrease with f. At lower f, the maximum mass $M_{\rm TOV}$ may exceeds $2.4\,M_\odot$. We also notice for both cases displayed in Fig. 7, $\Lambda_{1.4}$ lies in the range of GW170817 constraint [82]. In a word, there exists a large parameter space for f that the linked bag model predicts compact star structures satisfying the observational constraints on mass and tidal deformability.

IV. DISCUSSIONS AND CONCLUSIONS

It is a giant leap in fundamental physics to recognize microscopically that ordinary objects are composed by "uncuttable" atoms during the ancient Greece time of Democritus, but the interaction between atoms could not be understood until the era of quantum physics in which electrons could penetrate through the atoms, e.g., via quantum tunneling. In an analogy of this normal condensed (electric) matter, quarks propagate between the strong units (baryons or strangeons) may also introduce interaction for strong matter. In fact, this is understandable since a perturbative approach of quantum mechanics could usually result in a lower ground state than the "unperturbed" one, as is remarked in text books (for the ground state, the second-order shift is negative [84]), leading to an attractive interaction at long distances.

In this paper, we model the strong condensed matter of 3-flavoured strangeons with a linked bag approach. For fixed bag parameters B_2 and B_3, the model parameters C_1 and z_0 are calibrated by reproducing the saturation properties (E/A, K_0, $E_{\rm sym}$ and L) of nucleon matter. Beside these, a dampening factor f is introduced to account for the reduction of quark energy level corrections. The obtained energy per baryon of strangeon matter is usually smaller than that of nuclear and hyperonic matter, which can be further reduced if we adopt larger quark numbers ($N_{\rm q}$) inside a strangeon. The corresponding EOSs of strangeon matter become stiffer as well, which increases the maximum mass of strangeon stars. It is found that, for $N_{\rm q} = 9$, the maximum mass of strangeon stars could be $\sim 2.5M_\odot$, while the tidal deformability of a $1.4\,M_\odot$ strangeon star $\Lambda_{1.4} \simeq (180 \sim 340)$. To investigate the parameter dependence, the maximum mass and tidal deformability of strangeon stars predicted by the linked bag model are examined by adopting various B_2, B_3, and f, which are consistent with the current astrophysical constraints in a large parameter space. Nevertheless, more refined theoretical efforts are required in our future study, where the quark single particle energy [63], the interactions among quarks (instanton, electric and magnetic gluon exchange, etc.), the center-of-mass correction [85], the effects of color superconductivity [86, 87], the quark composition of strangeons, and the possible mixing of different types of strangeons and baryons should be examined carefully. Those effects could easily alter our

predictions on M_{TOV} and $\Lambda_{1.4}$ of strangeon stars, which should be tested further in the era of multi-messenger astronomy.

[1] A. Li, Z.-Y. Zhu, E.-P. Zhou, J.-M. Dong, J.-N. Hu, and C.-J. Xia, JHEAP (2020), 10.1016/j.jheap.2020.07.001.

[2] S. Weissenborn, I. Sagert, G. Pagliara, M. Hempel, and J. Schaffner-Bielich, Astrophys. J. 740, L14 (2011).

[3] T. Klähn, R. Łastowiecki, and D. Blaschke, Phys. Rev. D 88, 085001 (2013).

[4] T. Zhao, S.-S. Xu, Y. Yan, X.-L. Luo, X.-J. Liu, and H.-S. Zong, Phys. Rev. D 92, 054012 (2015).

[5] T. Kojo, P. D. Powell, Y. Song, and G. Baym, Phys. Rev. D 91, 045003 (2015).

[6] A. Li, W. Zuo, and G. X. Peng, Phys. Rev. C 91, 035803 (2015).

[7] K. Masuda, T. Hatsuda, and T. Takatsuka, Eur. Phys. J. A 52, 65 (2016).

[8] D. L. Whittenbury, H. H. Matevosyan, and A. W. Thomas, Phys. Rev. C 93, 035807 (2016).

[9] N.-U. F. Bastian, D. Blaschke, T. Fischer, and G. Röpke, Universe 4, 67 (2018).

[10] E. Annala, T. Gorda, A. Kurkela, J. Nättilä, and A. Vuorinen, Nat. Phys. (2020), 10.1038/s41567-020-0914-9.

[11] D. Blaschke, A. Ayriyan, D. E. Alvarez-Castillo, and H. Grigorian, Universe 6, 81 (2020).

[12] D. Blaschke and D. Alvarez-Castillo, Eur. Phys. J. A 56, 124 (2020).

[13] C.-J. Xia, T. Maruyama, N. Yasutake, T. Tatsumi, H. Shen, and H. Togashi, Phys. Rev. D 102, 023031 (2020).

[14] S. Weissenborn, D. Chatterjee, and J. Schaffner-Bielich, Phys. Rev. C 85, 065802 (2012).

[15] Bednarek, I., Haensel, P., Zdunik, J. L., Bejger, M., and Mańka, R., Astron. Astrophys. 543, A157 (2012).

[16] M. Oertel, C. Providência, F. Gulminelli, and A. R. Raduta, J. Phys. G: Nucl. Part. Phys. 42, 075202 (2015).

[17] K. Maslov, E. Kolomeitsev, and D. Voskresensky, Nucl. Phys. A 950, 64 (2016).

[18] T. Takatsuka, S. Nishizaki, and Y. Yamamoto, Eur. Phys. J. A 13, 213 (2002).

[19] D. Lonardoni, A. Lovato, S. Gandolfi, and F. Pederiva, Phys. Rev. Lett. 114, 092301 (2015).

[20] H. Togashi, E. Hiyama, Y. Yamamoto, and M. Takano, Phys. Rev. C 93, 035808 (2016).

[21] I. Vidaña, AIP Conf. Proc. 1645, 79 (2015).

[22] M. Fortin, S. S. Avancini, C. Providência, and I. Vidaña, Phys. Rev. C 95, 065803 (2017).

[23] T.-T. Sun, C.-J. Xia, S.-S. Zhang, and M. S. Smith, Chin. Phys. C 42, 25101 (2018).

[24] B. Holdom, J. Ren, and C. Zhang, Phys. Rev. Lett. 120, 222001 (2018).

[25] T.-T. Sun, S.-S. Zhang, Q.-L. Zhang, and C.-J. Xia, Phys. Rev. D 99, 023004 (2019).

[26] T. Zhao, W. Zheng, F. Wang, C.-M. Li, Y. Yan, Y.-F. Huang, and H.-S. Zong, Phys. Rev. D 100, 043018 (2019).

[27] C. Zhang, Phys. Rev. D 101, 043003 (2020).

[28] E. Witten, Phys. Rev. D 30, 272 (1984).

[29] P. Haensel, J. L. Zdunik, and R. Schaeffer., Astron. Astrophys. 160, 121 (1986).

[30] C. Alcock, E. Farhi, and A. Olinto, Astrophys. J. 310, 261 (1986).

[31] F. Weber, Prog. Part. Nucl. Phys. 54, 193 (2005).

[32] R.-X. Xu, Astrophys. J. 596, L59 (2003).

[33] W. Wang, J. Lu, H. Tong, M. Ge, Z. Li, Y. Men, and R. Xu, Astrophys. J. 837, 81 (2017).

[34] R. L. Jaffe, Phys. Rev. Lett. 38, 195 (1977); Phys. Rev. Lett. 38, 617 (1977).

[35] A. T. M. Aerts, P. J. G. Mulders, and J. J. de Swart, Phys. Rev. D 17, 260 (1978).

[36] K. Maltman, Phys. Lett. B 291, 371 (1992).

[37] Y. Maezawa, T. Hatsuda, and S. Sasaki, Prog. Theor. Phys. 114, 317 (2005).

[38] S. H. Lee and S. Yasui, Eur. Phys. J. C 64, 283 (2009).

[39] S. R. Beane, E. Chang, W. Detmold, B. Joo, H. W. Lin, T. C. Luu, K. Orginos, A. Parreño, M. J. Savage, A. Torok, and A. Walker-Loud (NPLQCD Collaboration), Phys. Rev. Lett. 106, 162001 (2011).

[40] T. Inoue, N. Ishii, S. Aoki, T. Doi, T. Hatsuda, Y. Ikeda, K. Murano, H. Nemura, and K. Sasaki (HAL QCD Collaboration), Phys. Rev. Lett. 106, 162002 (2011).

[41] K. Sasaki, S. Aoki, T. Doi, S. Gongyo, T. Hatsuda, Y. Ikeda, T. Inoue, T. Iritani, N. Ishii, K. Murano, and T. Miyamoto, Nucl. Phys. A 998, 121737 (2020).

[42] T. Sakai, J. Mori, A. Buchmann, K. Shimizu, and K. Yazaki, Nucl. Phys. A 625, 192 (1997).

[43] N. K. Glendenning and J. Schaffner-Bielich, Phys. Rev. C 58, 1298 (1998).

[44] X. Y. Lai, C. Y. Gao, and R. X. Xu, Mon. Not. R. Astron. Soc. 431, 3282 (2013).

[45] R. Xu, Sci. China-Phys. Mech. Astron. 61, 109531 (2018).

[46] J. E. Horvath, Mod. Phys. Lett. A 20, 2799 (2005).

[47] B. J. Owen, Phys. Rev. Lett. 95, 211101 (2005).

[48] M. Mannarelli, K. Rajagopal, and R. Sharma, Phys. Rev. D 76, 074026 (2007).

[49] X. Lai and R. Xu, J. Phys: Conf. Ser. 861, 012027 (2017).

[50] X. Lai, E. Zhou, and R. Xu, Eur. Phys. J. A 55, 60 (2019).

[51] X.-Y. Lai, C.-J. Xia, and R.-X. Xu, "Merging strangeon stars: the ejecta and light curves," (2020), private communication.

[52] P. J. Mulders, A. T. Aerts, and J. J. de Swart, Phys. Rev. D **21**, 2653 (1980).

[53] K. Liu and C. Wong, Phys. Lett. B **113**, 1 (1982).

[54] M. Oka, K. Shimizu, and K. Yazaki, Phys. Lett. B **130**, 365 (1983).

[55] U. Straub, Z.-Y. Zhang, K. Brauer, A. Faessler, and S. Khadkikar, Phys. Lett. B **200**, 241 (1988).

[56] M. Oka and S. Takeuchi, Nucl. Phys. A **524**, 649 (1991).

[57] P. Shen, Z. Zhang, Y. Yu, X. Yuan, and S. Yang, J. Phys. G **25**, 1807 (1999).

[58] A. P. Balachandran, A. Barducci, F. Lizzi, V. G. J. Rodgers, and A. Stern, Phys. Rev. Lett. **52**, 887 (1984).

[59] R. Jaffe and C. Korpa, Nucl. Phys. B **258**, 468 (1985).

[60] S. A. Yost and C. R. Nappi, Phys. Rev. D **32**, 816 (1985).

[61] V. Kopeliovich, B. Schwesinger, and B. Stern, Nucl. Phys. A **549**, 485 (1992).

[62] A. Chodos, R. L. Jaffe, K. Johnson, C. B. Thorn, and V. F. Weisskopf, Phys. Rev. D **9**, 3471 (1974).

[63] Q.-R. Zhang and H.-M. Liu, Phys. Rev. C **46**, 2294 (1992).

[64] T. DeGrand, R. L. Jaffe, K. Johnson, and J. Kiskis, Phys. Rev. D **12**, 2060 (1975).

[65] E. S. Fraga and P. Romatschke, Phys. Rev. D **71**, 105014 (2005).

[66] M. S. Berger and R. L. Jaffe, Phys. Rev. C **35**, 213 (1987).

[67] M. S. Berger and R. L. Jaffe, Phys. Rev. C **44**, 566 (1991).

[68] J. Madsen, Phys. Rev. D **50**, 3328 (1994).

[69] J. Vermaseren, S. Larin, and T. van Ritbergen, Phys. Lett. B **405**, 327 (1997).

[70] E. S. Fraga, A. Kurkela, and A. Vuorinen, Astrophys. J. **781**, L25 (2014).

[71] E. Shuryak, Phys. Lett. B **79**, 135 (1978).

[72] S. Shlomo, V. M. Kolomietz, and G. Colò, Eur. Phys. J. A **30**, 23 (2006).

[73] B.-A. Li and X. Han, Phys. Lett. B **727**, 276 (2013).

[74] M. Oertel, M. Hempel, T. Klähn, and S. Typel, Rev. Mod. Phys. **89**, 015007 (2017).

[75] European Muon Collaboration, Phys. Lett. B **123**, 275 (1983).

[76] J. W. Negele and D. Vautherin, Nucl. Phys. A **207**, 298 (1973).

[77] G. Baym, C. Pethick, and P. Sutherland, Astrophys. J. **170**, 299 (1971).

[78] J. Lu, E. Zhou, X. Lai, and R. Xu, Sci. China Phys. Mech. Astron. **61**, 089511 (2018).

[79] P. B. Demorest, T. Pennucci, S. M. Ransom, M. S. E. Roberts, and J. W. T. Hessels, Nature **467**, 1081 (2010).

[80] E. Fonseca, T. T. Pennucci, J. A. Ellis, I. H. Stairs, D. J. Nice, S. M. Ransom, P. B. Demorest, Z. Arzoumanian, K. Crowter, T. Dolch, R. D. Ferdman, M. E. Gonzalez, G. Jones, M. L. Jones, M. T. Lam, L. Levin, M. A. McLaughlin, K. Stovall, J. K. Swiggum, and W. Zhu, Astrophys. J. **832**, 167 (2016).

[81] J. Antoniadis, P. C. C. Freire, N. Wex, T. M. Tauris, R. S. Lynch, M. H. van Kerkwijk, M. Kramer, C. Bassa, V. S. Dhillon, T. Driebe, J. W. T. Hessels, V. M. Kaspi, V. I. Kondratiev, N. Langer, T. R. Marsh, M. A. McLaughlin, T. T. Pennucci, S. M. Ransom, I. H. Stairs, J. van Leeuwen, J. P. W. Verbiest, and D. G. Whelan, Science **340**, 1233232 (2013).

[82] LIGO Scientific and Virgo Collaborations, Phys. Rev. Lett. **121**, 161101 (2018).

[83] LIGO Scientific and Virgo Collaborations, Astrophys. J. **896**, L44 (2020).

[84] F. Schwabl, *Quantum Mechanics* (Springer-Verlag Berlin Heidelberg, 2007).

[85] J. Bartelski, A. Szymacha, L. Mankiewicz, and S. Tatur, Phys. Rev. D **29**, 1035 (1984).

[86] M. Buballa, Phys. Rep. **407**, 205 (2005).

[87] M. G. Alford, A. Schmitt, K. Rajagopal, and T. Schäfer, Rev. Mod. Phys. **80**, 1455 (2008).